Dynamics of the $O(^3P)+HCl$ reaction on the $^3A''$ electronic state: A new *ab initio* potential energy surface, quasi-classical trajectory study, and comparison to experiment

B. Ramachandran and Ethan A. SchraderIII
Chemistry, College of Engineering and Science, Louisiana Tech University, Ruston, Louisiana 71272

Jörg Senekowitsch
Friedrichstrasse 23, 61440 Oberursel, Germany

Robert E. Wyatt
Department of Chemistry and Biochemistry, University of Texas, Austin, Texas 78712

(Received 12 April 1999; accepted 8 June 1999)

A new potential energy surface for the lowest $^3A''$ electronic state of the $O(^3P)+HCl$ system is presented. This surface is based on electronic energies calculated at the multireference configuration interaction level of theory with the Davidson correction (MR-CI+Q) using the Dunning cc-pVTZ one-electron basis sets. The *ab initio* energies thus obtained are scaled using the scaled external correlation (SEC) method of Brown and Truhlar. The SEC-scaled energies are fitted to a simple analytical expression to yield a potential energy surface which correlates the reactants $O(^3P)+HCl(^1\Sigma^+)$ to the products $OH(^2\Pi)+Cl(^2P)$. The reaction barrier on this surface lies at an O–H–Cl angle of 131.4° at an energy of 9.78 kcal/mol above the asymptotic O+HCl minimum. This barrier is 1.3 kcal/mol higher than that on the potential energy surface obtained by Koizumi, Schatz, and Gordon (KSG) [J. Chem. Phys. **95**, 6421 (1991)] and 1.1 kcal/mol lower than the S2 surface of Ramachandran, Senekowitsch, and Wyatt (RSW) [J. Mol. Struct. (Theochem) **454**, 307 (1998)]. The dynamics of the reaction $O(^3P)+HCl(v=2;\ j=1,6,9)\rightarrow OH(v',j')+Cl$ on this potential surface is studied using quasi-classical trajectory (QCT) propagation and the results are compared to the experimental observations of Zhang *et al.* [R. Zhang, W. J. van der Zande, M. J. Bronikowski, and R. N. Zare, J. Chem. Phys. **94**, 2704 (1991)]. The broad distribution of collision energies in the experiment is modeled by computing weighted averages of the quantities of interest with the weighting factor at each collision energy determined by the collision energy distribution. © *1999 American Institute of Physics.* [S0021-9606(99)02333-8]

I. INTRODUCTION

The reaction of $O(^3P)$ with HCl plays an important role in the chemistry of the stratospheric ozone layer.[1] It is also a heavy-light-heavy type reaction amenable to both experimental and theoretical study.[2] It is not surprising, therefore, that there have been many experimental studies of this reaction, which range from measurements of the thermal[3–14] and reagent state-resolved[15–19] rate coefficients to the determination of state-to-state integral cross sections.[20,21] The theoretical studies of this reaction, to be detailed below, have ranged from estimation of thermal rate coefficients using transition state theory and quasiclassical trajectory (QCT) methods to extensive quantum mechanical calculations.

Theoretical investigations of this reaction prior to the early nineties were carried out using model potential energy surfaces constructed under the assumption that the minimum energy saddle point corresponded to a collinear O–H–Cl geometry.[22–25] In 1989, the *ab initio* investigations of Gordon *et al.*[26] established that the minimum energy saddle point for this reaction, which lies on the lowest $^3A''$ electronic state, corresponds to a bent geometry. As a continuation of this work, Koizumi, Schatz, and Gordon (KSG)[27] constructed the first realistic potential energy surface for this system by fitting an extended LEPS model to scaled *ab initio* energies calculated at the MP2/6-31G(d, p) level of theory. The scaling of the *ab initio* energies were done in order to bring the approximate (total angular momentum $J=0$) quantum thermal rate coefficient into good agreement with the experimental value at 293 K.[27] The KSG potential energy surface thus obtained has a minimum energy saddle point at an O–H–Cl angle of 133.4°, at an energy of 8.5 kcal/mol above the asymptotic O+HCl minimum. This reaction barrier has been shown to be too low by more recent, and more extensive quantum mechanical calculations.[28–33]

This paper presents a new potential energy surface for the $1\ ^3A''$ electronic state of the $O(^3P)+HCl$ system and a quasiclassical trajectory simulation of the experiments of Zhang *et al.*[21] on this surface. This work is a continuation of the efforts of Ramachandran, Senekowitsch, and Wyatt (RSW)[34,35] to construct a realistic potential energy surface for this reaction, which has led to a series of fits to scaled *ab initio* data culminating in the one presented below. Previous published fits, denoted as S1, S1A, and S2, were determined to have reaction barriers that were too high (ranging from 10.03 to 10.98 kcal/mol) and too ''thick'' in the sense of not permitting enough tunneling at low temperatures.[35] These

conclusions were based on variational transition state theory[36] calculations using the improved canonical variational theory (ICVT)[37] with the microcanonical multidimensional tunneling correction (μOMT).[38] In fact, these calculations indicated that the KSG surface established a lower limit for the correct barrier height whereas the RSW surfaces established an upper limit. This work presents a new scaling and fit of the *ab initio* data that yields a barrier height between the KSG and RSW limits which, based on preliminary calculations of VTST thermal rate coefficients,[39] appears to be very close to the actual barrier.

It is well-known that the temperature dependence of thermal rate constants is not particularly sensitive to the finer details of the potential energy surface. For instance, some of the model surfaces used in earlier attempts to study this reaction yielded very good agreement of QCT and experimental thermal rate coefficients[22,23] in spite of the wrong saddle point geometry. Recently, however, thanks to the pioneering work from the laboratory of Zare,[20,21] experimental state-to-state integral cross sections for the elementary reactions $O(^3P)+HCl(v=2;j=1,6,9)\rightarrow OH\ (v'=0,1;j')+Cl$ have become available. Product rotational distributions depend sensitively on the nature of the three-body interaction potential and, due to the relatively high total energies involved in this case, their theoretical reproduction depends not only on the correct position and height of the reaction barrier but also on the accurate representation of the potential at geometries quite far from the minimum energy path.

One of the main motivations for our attempts to generate an accurate potential energy surface for this reaction has been the desire to account for the rather unique, nonmonotonic rise in product rotational state populations in the OH ($v'=0$) manifold observed in the experiments of Zhang *et al.*[21] The observed product rotational distributions from the HCl ($v=2;j=1,6$) clearly show a two peak structure, with a low amplitude peak occurring at $j'=10$, followed by a rather dramatic dip at $j'=11$ and then a rapid, monotonic rise to the j' state with the highest population. This structure in the rotational distributions becomes less pronounced as the initial j quantum number increases, and reduces to a ''shoulder'' in the case of reactions initiated in the $(v,j)=(2,9)$ state of HCl. This type of structure is, of course, rather unusual (in fact, initially the experimentalists did not trust their results[40]) and, therefore, a potential energy surface that can account for it can provide valuable insight into the reaction dynamics responsible for it.

Our first attempt at modeling the reactions of $O(^3P)$ with HCl ($v=2;j=1,6,9$) using the QCT method on the S1 surface[34] did, in fact, reproduce the bimodal distribution observed in the experiments. However, these calculations were done at a single collision energy (3.2 kcal/mol, the average collision energy in the experiments of Zhang *et al.*) and used a small ensemble of trajectories (20 000 per initial state). It was discovered later that calculations which accumulated better statistics and included the distribution of collision energies present in the experiment averaged out the structure in the rotational distributions. The bimodal rotational distributions could not be reproduced using QCT dynamics on the S1A and S2 surfaces. The recent work of Aoiz *et al.*[33] shows that the QCT rotational distributions on the KSG surface also show no indication of the observed structure in product rotational distributions. On the other hand, the QCT results on the potential energy surface presented here clearly shows a bimodal structure in the OH($v'=0$) rotational distributions for reactions initiated in the HCl ($v=2,j=1$) state, and a broad shoulder in this region for the other two initial states, even when the collision energy distribution is taken into account. Moreover, at collision energies close to the average value of 3.2 kcal/mol reported by Zhang *et al.*, the present surface yields OH ($v'=0$) rotational distributions that bear striking qualitative similarities to the experimental distributions for the other two initial states.

It should be noted that, in spite of the recent advances in atom-molecule reactive scattering calculations using quantum mechanics, a completely quantum mechanical treatment of this reaction to obtain product rotational distributions comparable to the experimental results is still very difficult. The most extensive quantum calculations to date for this reaction are those of Nakamura and co-workers[28,30] on the KSG potential surface. These calculations, which employ the extended constant centrifugal potential approximation (CCPA) in order to keep the computational effort manageable, show that total angular momentum quantum numbers up to $J\approx 120$ have to be considered in order to converge the reaction cross sections out of HCl ($v=0,j=0-10$) for collision energies less than 0.70 eV (internal energies $\leqslant 0.33$ eV). The even higher total energies required to access the HCl $v=2$ states probed in the experiments (internal energies are between 0.9 and 1.1 eV) may further increase the upper limit of the total angular momentum quantum number that must be included.

On the other hand, quasiclassical trajectory (QCT) methods can easily deal with this reaction without additional simplifying approximations. The work of Aoiz and co-workers[41–45] has shown that, provided sufficiently large numbers of trajectories can be computed and good statistics compiled, the QCT method can reproduce many of the details of the quantum mechanical calculations even for highly ''quantum mechanical'' systems such as $D+H_2$ with nearly quantitative accuracy. Obviously, the QCT method cannot be expected to be reliable at energies near the reaction threshold where barrier penetration and tunneling through vibrationally adiabatic effective potentials may play important roles. However, the reactions studied in the Zare experiments occur at energies well above the reaction barrier and are, therefore, likely to be essentially free from such quantum mechanical effects. Further, it has been observed that QCT results for vibrationally excited reagents in the $D+H_2$ reaction[44] and the Li+HF reaction[45] are in much better agreement with quantum calculations than those for the vibrationally unexcited reagents.

The remainder of this paper is organized as follows: In Sec. II, we present the details of the computations for the potential surface, the model used for its analytical representation, and examine the general topographic features of the potential and check the accuracy of the fit. This section also summarizes the details of the quasiclassical trajectory calculations including the modeling of the collision distributions

present in the experiments. In Section III, the results of these calculations are analyzed and compared to the experimental results of Zhang *et al.*[21] Section IV is a discussion of this work.

II. CALCULATIONS

A. *Ab initio* energies and the scaling procedure

The potential energy surface for the $1\,^3A''$ state, correlating $O(^3P)+HCl(\tilde{X}\,^1\Sigma^+)$ to $OH(^2\Pi)+Cl(^2P)$, is based on scaled *ab initio* energies obtained using the MOLPRO92 package of programs[46] at the MR-CISD level of theory. These calculations used full valence CASSCF wave functions as references, and employed the internally contracted CI algorithm of Werner and Knowles.[47] The correlation consistent polarized valence triple zeta (cc-pVTZ) basis sets of Dunning[48] were used, which resulted in a basis of H $(5s2p1d)/[3s2p1d]$, O $(10s5p2d1f)/[4s3p2d1f]$, and Cl $(15s9p2d1f)/[5s4p2d1f]$, amounting to 78 symmetry adapted contracted Gaussian basis functions. The atomic core orbitals for the CASSCF calculations were initially obtained by closed shell Hartree–Fock calculations on the double anion $HClO^{2-}$. An additional CASSCF run was then made to relax the core orbitals, which were still treated as closed shells, and the resulting molecular orbitals used as references for the MRCI calculations. The CI calculations correlated all fourteen valence electrons, but did not include the effects of core-valence correlation.

As described in Ref. 34, the MRCI energies lead to a potential surface on which the reaction barrier is too high. This was verified by a few QCT calculations in which trajectories were initiated in the HCl $v=2, j=1,6,9$ states at collision energies of 3.2 kcal/mol, the average collision energy estimated by Zhang *et al.*[21] in their experiments. The reaction probability on the MR-CISD surface for these initial states were found to be less than 2×10^{-4} (no reactive events from ensembles of 5000 trajectories for each initial state). In order to lower the reaction barrier without resorting to arbitrary scaling procedures, we first examined the Davidson corrected energies (MR-CI+Q)[49,50] which are also computed by the CI program in MOLPRO92. It was found that an even further lowering of the reaction barrier was required, and this was achieved by scaling the MR-CI+Q energies based on the difference between the CASSCF and MRCI+Q energies at each geometry.[34] This is essentially the same as the Scaled External Correlation (SEC) method of Brown and Truhlar,[51] where the scaling is based on the difference between the CASSCF and MRCI energies.

The SEC method[51] is a semiempirical technique that attempts to account for all of the dynamical correlation energy remaining unrecovered after a CAS/CI calculation. The assumptions made are that (a) the core correlation energy is independent of the molecular geometry, (b) a ''reasonably large one-electron basis set'' will account for almost all of the geometry-dependent nondynamical correlation energy in the multiconfiguration SCF calculation, (c) the difference between the MCSCF or full valence CASSCF energy and the MR-CISD energy provides a measure of the missing dynamical correlation energy, and (d) the dynamical correlation energy is independent of geometry and can be expressed as a constant (i.e., geometry independent) fraction of the difference between the CAS and CI energies. In contrast to the Davidson correction, which is based on the expansion coefficients of the CI wave function, the SEC procedure uses empirical information, typically experimental dissociation energies of the diatomic fragments, to estimate the fraction of the ''external'' or dynamical correlation energy unrecovered by the CI calculation. The SEC method has been used to develop potential energy surfaces for the $F+H_2$,[52,53] $Cl+H_2$,[54] and, more recently, the $O(^3P)+HCl$ reactions.[34,35] In the case of the $O(^3P)+HCl$ system, as explained above, we scale the CI+Q energies in essentially the same manner. The SEC scaled CI+Q energies, denoted here as CI+Q/SEC, are obtained as

$$E_{\mathrm{CI+Q/SEC}}=E_{\mathrm{CAS}}+\frac{(E_{\mathrm{CI+Q}}-E_{\mathrm{CAS}})}{F}, \tag{1}$$

where the scaling factor F is determined from calculated diatomic dissociation energies, as

$$F_{AB}=\frac{D_{e,AB}^{\mathrm{CI+Q}}-D_{e,AB}^{\mathrm{CAS}}}{D_{e,AB}^{\mathrm{Expt.}}-D_{e,AB}^{\mathrm{CAS}}}, \tag{2}$$

where the D_e's are the dissociation energies at the indicated level of theory. In the case of the S1, S1A, and S2 surfaces mentioned earlier, the factor F appearing in Eq. (1) was obtained as the average of F_{HCl} and F_{OH}. The scaling factor for the present potential surface is obtained as[55]

$$F=\tfrac{1}{3}(F_{\mathrm{HCl}}+F_{\mathrm{OH}}+F_{\mathrm{ClO}}). \tag{3}$$

The most important difference between the surfaces S1-S2 and the present one is in the magnitude of the scaling factor F. It is obvious from above that the smaller the value of F, the more dramatic the effects of the scaling. The magnitude of F depends inversely on the amount of dynamical correlation energy that remains unrecovered at the CASSCF stage, a quantity that depends very strongly on the molecule studied and the completeness of the one-electron basis. In the course of these calculations, it became rather obvious that it was especially difficult to extract correlation energy from the ClO fragment. Therefore, compared to the HCl and OH molecules, the scaling factor calculated in Eq. (2) for ClO was considerably smaller. This has the effect of lowering the average scaling factor and hence the barrier height on the surface. A recent calculation on the $\tilde{X}\,^1A'$ state of the HOCl molecule using the significantly larger ''augmented'' cc-pVTZ (cc-pAVTZ) basis set yielded much larger diatomic dissociation energies at all levels of theory and, therefore, a larger average value for F.[56]

B. The S4 potential energy surface

The potential energy surface presented here is based on a set of 463 scaled *ab initio* points calculated over a nonuniform grid in $\{r_{\mathrm{OH}}, r_{\mathrm{HCl}}, \theta_{\mathrm{OHCl}}\}$ in the ranges $1.25a_0 \leqslant R_{\mathrm{OH}} \leqslant 6.0a_0$, $1.75a_0 \leqslant R_{\mathrm{HCl}} \leqslant 6.5a_0$, at θ_{OHCl} values of 70, 90, 110, 130, 150, and 170° and a smaller grid spanning the saddle point region at $\theta_{\mathrm{OHCl}}=125,135,140$, and 175°. The H+ClO channel does not become energetically accessible

until the total energy exceeds 42.0 kcal/mol measured from the asymptotic O+HCl minimum and, therefore, was not included in the fit for the present surface. Since no *ab initio* points were computed for $\theta_{OHCl}<70°$, at 20° intervals in the range $10°\leqslant\theta_{OHCl}<90°$, in the vicinity of the appropriate r_e value, we placed 5 points generated from each of the two body terms (a total of 10 points per angle) at a distance of $10a_0$ from the third atom, in order to ''guide'' the fit. This was found to be necessary to avoid unphysical behavior of the fit at short internuclear distances. These 503 points were fit to a many body type expansion given by

$$V(r_{OH},r_{HCl},r_{ClO})=V^{(2)}(r_{OH})+V^{(2)}(r_{HCl})+V^{R}(r_{ClO})+V^{(3)}(r_{OH},r_{HCl},\theta_{OHCl}). \quad (4)$$

In this expression, the total energy of the three atoms at infinite separation is set to zero. The two body potentials $V^{(2)}$ were provided by the bond-order expansion of Garcia and Laganá[57]

$$V^{(2)}(r)=-D_e\sum_{i=1}^{N} c_i\eta^i, \quad (5)$$

where $\eta=\exp[-\beta(r-r_e)]$ and $N=4$. In order to guarantee that this expansion has a minimum equal to $-D_e$ at $r=r_e$, the expansion coefficients were forced to satisfy the following conditions:

$$\sum_{i=1}^{N} c_i=1; \quad \sum_{i=1}^{N} ic_i=0. \quad (6)$$

The linear parameters c_i and the nonlinear parameter β were found by requiring the ω_e and $\omega_e x_e$ values for each diatomic to be equal to their experimental values[58] following the procedure of Garcia and Laganá.[57] This procedure, combined with the restrictions in Eq. (6) yields identical coefficients $\{c_i\}$ for all molecules. The terms with c_1 and c_3 account for the attractive part of the potential while the terms with c_2 and c_4 represent the repulsive part. Note that for the case $N=2$, this model reduces to the Morse expression, with $c_1=2$ and $c_2=-1$. The r_e value for each diatomic was set equal to the value found by fitting scaled *ab initio* data during the construction of surface S1.[34] A repulsive potential V^R was also introduced to prevent the unphysical situation of Cl and O atoms approaching each other without experiencing any repulsive force. This potential has the form

$$V^{R}(r)=-D_e[c_2\eta+c_4\eta^2]. \quad (7)$$

Note that the powers of the variable η have been reduced from the values of 2 and 4 suggested by Eq. (5) to increase the range of the repulsive potential. This was found to be necessary to avoid unphysical wells at intermediate (r_{OH},r_{HCl}) values for $\theta_{OHCl}<70°$.

The three body term was expanded in coordinates similar to the one introduced by Aguado and Paniagua,[59] and the cosine of the O–H–Cl angle, as

$$V^{(3)}=\sum_{j,k=1}^{6}\sum_{l=0}^{7} C_{jkl}\rho_{OH}^{j}\rho_{HCl}^{k}\cos^{l}(\theta_{OHCl}); \quad j+k+l\leqslant 9 \quad (8)$$

where $\rho=r\exp[-\alpha(r-r_e)]$, and the parameter α was fixed at 0.75β after some numerical experimentation. This expansion resulted in 112 linear parameters C_{jkl} whose optimal values were found using standard methods. The root-mean-square error of the fit is 0.48 kcal/mol. The minimum energy saddle point separating the reactants from the products was located at $(r_{OH}^{\ddagger},r_{HCl}^{\ddagger})=(2.42a_0,2.66a_0)$ and $\theta_{OHCl}=131.4°$ at an energy of 9.78 kcal/mol above the asymptotic O+HCl minimum. There is a secondary saddle point, located at $(r_{OH}^{\ddagger},r_{HCl}^{\ddagger})=(2.26a_0,2.72a_0)$ and $\theta_{OHCl}=180°$, at an energy of 12.95 kcal/mol. The structural and spectroscopic properties of these saddle points are compared to those on the S1, S1A, S2, and KSG surfaces in Table I. In this Table, the subscripts to the vibrational frequencies indicate the symmetric stretch, bend, and asymmetric stretch modes, the last of which is imaginary at the saddle point. The barrier heights reported are the classical barrier height $\Delta V^{\ddagger}$ and the barrier height corrected for the zero point energies (zpe) of the reactant and the saddle point, $\Delta V_{zpe}^{\ddagger}$.

TABLE I. Saddle point properties of the potential energy surfaces available for the $^3A''$ state.

	S1	S1A	S2	S4	KSG
$r_{HCl}^{\ddagger}(a_0)$	2.712	2.687	2.691	2.664	2.620
$r_{OH}^{\ddagger}(a_0)$	2.372	2.382	2.394	2.416	2.328
$\theta_{OHCl}^{\ddagger}$(deg.)	132.1	134.6	132.9	131.4	133.4
$\omega_s^{\ddagger}(cm^{-1})$	1446	1395	1408	1523	1332
$\omega_b^{\ddagger}(cm^{-1})$	316	309	267	290	429
$\omega_a^{\ddagger}(cm^{-1})$	1537*i*	1603*i*	2042*i*	1619*i*	1337*i*
$\Delta V^{\ddagger}$(kcal/mol)	10.03	10.32	10.98	9.78	8.50
$\Delta V_{zpe}^{\ddagger}$(kcal/mol)	8.47	8.30	9.10	8.13	6.75

Prior to obtaining this fit, we had attempted to construct a ''global'' surface using a slightly different model by including 80 scaled *ab initio* points leading from the three-body interaction region towards the asymptotic H+ClO region in the dataset used for the fit. However, all attempts to produce a physically reasonable surface employing a reasonably small number of linear parameters and acceptably low rms error failed. A fit using 120 linear parameters did yield a low rms error ($\simeq$0.5 kcal/mol), but warnings about false convergence and possible discontinuities in parameter space were generated during the fitting procedure. Moreover, QCT modeling of the experiments of Zhang *et al.*[21] on the resulting fit, which we called the S3 surface, yielded product rotational distributions that were too ''cold'' by 2-4 rotational quanta. Therefore, we abandoned those attempts and proceeded to construct the present surface, which we call the S4 surface.

Contour plots of the S4 surface at four values of θ_{OHCl} are shown in Fig. 1. The panel Fig. 1(a) shows that even at $\theta_{OHCl}=10°$, where no *ab initio* points are present in the dataset used for the fit, the surface remains physically reasonable, once allowance is made for the fact that the H+ClO arrangement is absent. The repulsive contribution from the term V^R is clearly visible at this angle, preventing communication between the entrance and exit channels. Of particular interest in panels (b) and (d) of Fig. 1 are, respectively, the wells on the product side of the barrier at $\theta_{OHCl}=80.4°$

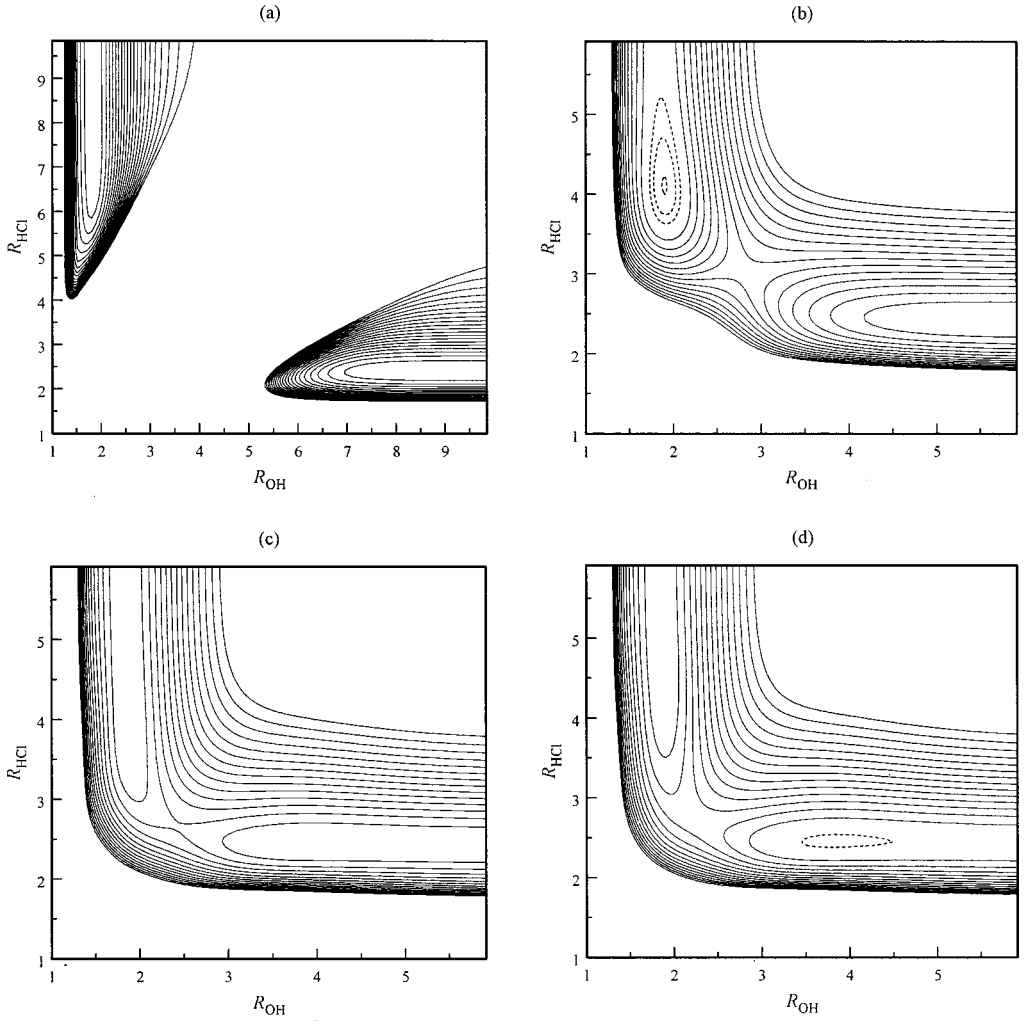

FIG. 1. Contours of the S4 surface at O–H–Cl angles of (a) 10°, (b) 80.4°, (c) 131.4°, and (d) 180°. The dashed contour lines represent negative values with respect to the asymptotic entrance channel minimum. The contours are drawn at -5, -3, -1 kcal/mol and in increments of 5 kcal/mol from 5 to 100 kcal/mol in panel (a) and from 5 to 70 kcal/mol in the other three panels.

and on the reactant side of the barrier at $\theta_{OHCl}=180°$. From the calculations of Allison *et al.*,[39] the minimum of the entrance channel well is located at $(r_{OH},r_{HCl})=(3.83a_0,2.46a_0)$ at $\theta_{OHCl}=180°$, while the exit channel well minimum is located at $(r_{OH},r_{HCl})=(1.90a_0,4.12a_0)$ at $\theta_{OHCl}=80.4°$. The depths of these two minima with respect to the asymptotic entrance channel minimum energy are, respectively, -1.64 and -5.18 kcal/mol.

An examination of the angular dependence of the potential with (r_{OH},r_{HCl}) fixed at their saddle point values is presented in Fig. 2(a). *Ab initio* points at 10° intervals in $90° \leqslant \theta_{OHCl} \leqslant 170°$ at the CAS, CI, and CI+Q levels of theory as well as the corresponding CI+Q/SEC energies are shown as symbols. The origin of the energy axis has been adjusted so that in each case, the energy plotted is the relative energy with respect to the asymptotic $O(^3P)+HCl$ minimum at the level of theory considered. In the case of the CAS, CI and CI+Q energies, the symbols are connected by smooth lines to guide the eye. In the case of the CI+Q/SEC energies, the comparison is made to the fit itself. The dashed lines above and below the solid line representing V calculated from Eq. (4) indicate the range defined by $V\pm\Delta V_{rms}$. It is clear that although the fit does not pass exactly through every scaled *ab initio* point, all of them do lie within the error of the fit. The angular dependence of the potential with (r_{OH},r_{HCl}) fixed at the values corresponding to the minimum of the well in the exit channel is shown in Fig. 2(b). The format is the same as that of Fig. 2(a). Once again, most of the scaled *ab initio* points are found lie within the error of the fit, although the agreement is not quite as good as that in Fig. 2(a). The scaled *ab initio* point at $\theta_{OHCl}=80°$ lies just inside the line representing $V-\Delta V_{rms}$, at -5.60 kcal/mol. Although not shown, a similar quality of agreement between scaled *ab initio* points and the values calculated from the fit is also observed for the entrance channel well for $\theta_{OHCl} \leqslant 175°$.

Two points need to be emphasized about these comparisons. The first one is that the *ab initio* points, represented as symbols in the panels of Fig. 2, were calculated *a posteriori*, i.e., after the fit was already obtained. Since these points were not part of the dataset used for the fit, these comparisons provide a stringent test of the quality of the surface. The second observation has to do with the role of dynamical correlation energy in determining the location as well as the energy of the points of interest. Panel (a) of Fig. 2 reveals

that not only the height, but also the location of the saddle point is affected by the extent of recovery of correlation energy. At the CAS level of theory, the minimum energy point in the angular dependence curve appears to lie between θ_{OHCl} angles of 150 and 160°. At CI and CI+Q levels of theory, the location of this point has shifted to $\theta_{\mathrm{OHCl}} \simeq 140°$, and the SEC scaling of the CI+Q energies further decreases the angle to 131.4°. Gordon *et al.*[26] also found that at the HF level, the saddle point for this system lies at a collinear geometry, but that recovery of correlation energy at post-HF levels of theory [e.g., MP2 and CCSD(T)] leads to the bent minimum energy saddle point. A similar dependence of the exit channel van der Waals minimum on correlation energy is seen in the case of the curves plotted in Fig. 2(b). The well in the exit channel is present only in the CI, CI+Q, and the CI+Q/SEC curves, indicating that these minima are described only through the recovery of dynamical correlation energy. As in the case of the saddle point, the SEC scaling of the CI+Q energies appear to shift the location of the minimum from about 82° to a value closer to 80°.

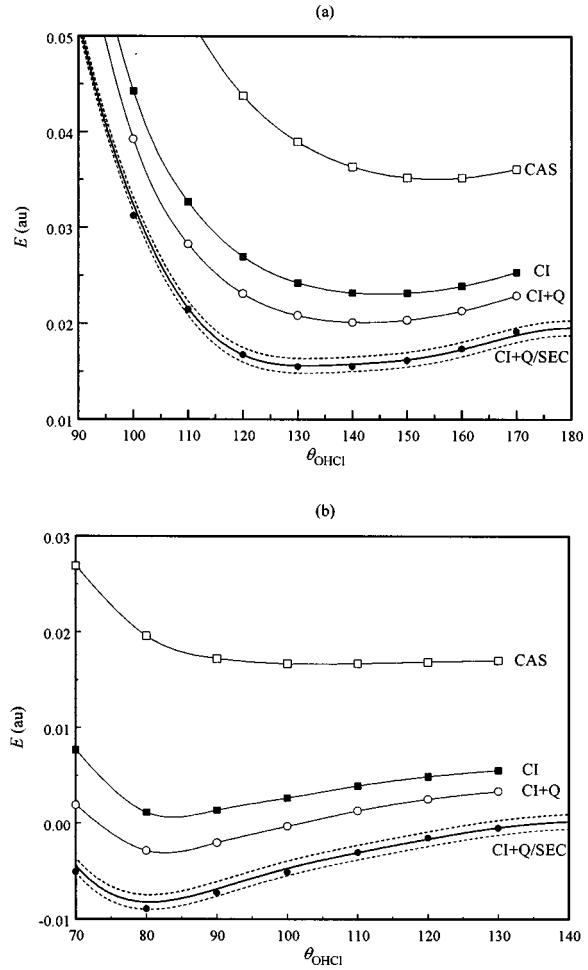

FIG. 2. The angular dependence of the potential at (a) the saddle point values of (r_{OH},r_{HCl}) and (b) at the values of (r_{OH},r_{HCl}) corresponding to the minimum in Fig. 1(b). Smooth lines connect the *ab initio* data at the CAS, CI, and CI+Q levels of calculation. The CI+Q/SEC data are compared to the fitted surface itself, shown as the solid line, with the dashed lines above and below representing the limits $V \pm \Delta V_{\mathrm{rms}}$.

C. Quasiclassical trajectory calculations

Our quasiclassical trajectory propagation code is based on Muckerman's program CLASTR, a version of which is available as Program No. 229 of the Quantum Chemistry Program Exchange (QCPE). The program is based on the approach outlined in Refs. 60 and 61. The accuracy of the numerical integration of the trajectories was verified by the standard methods of monitoring the conservation of total energy and angular momentum as well as back-integrating a few trajectories at each energy. The optimal value for the maximum impact parameter, b_{max}, was found to be 3.0 Å for the range of energies used in these calculations[62] although at one or two energies, a b_{max} value of about 3.1 Å was required to capture all reactive trajectories initiated in the HCl $(v,j)=(2,6)$ state. In the present set of calculations, 10 000 trajectories were initiated from each HCl initial state examined by the experiments of Zhang *et al.*, at collision energies ranging from 0.30 kcal/mol to a maximum of 11.0 kcal/mol. The collision energy was scanned in steps of 0.10 kcal/mol in the interval $0.3 < E_{\mathrm{coll}} < 1.0$ and in steps of 0.5 kcal/mol in the interval $1.0 < E_{\mathrm{coll}} < 11.0$ kcal/mol. A maximum of 280 000 trajectories were propagated from each initial state or, in other words, 10 000 trajectories for each initial state at each of the 28 collision energies examined.

As stated in the Introduction, one of the aims of these calculations is to compare the QCT product rotational distributions to those observed in the experiments of Zhang *et al.* The O(^3P) in these experiments were generated by photolysis of NO_2 at 355 nm. The photofragment imaging experiments of Hradil *et al.*[63] show that the O atom velocity distribution from laser photolysis of NO_2 at 355 nm has two peaks centered at 900 and 1400 m s^{-1} corresponding, respectively, to the formation of the $v=1$ and the $v=0$ states of the NO molecule. The HCl molecules in the experiment can be assumed to have the thermal velocity distribution given by the Maxwell–Boltzmann distribution. It is now well-recognized that the spread in the velocity distributions of the photolytic precursor (in this case, NO_2) as well as the target (HCl) has very profound effects on the distribution of collision energies in the O(^3P)+HCl reaction.[64–67] Taking these effects into account gives rise to ''superthermal'' widths[64] to the collision energy distributions. In order to mimic the distribution of collision energies in the experiments of Zhang *et al.*, we have used a collision energy distribution function nearly identical to the one used by Aoiz *et al.*[33] in a recent study of this reaction on the KSG surface. This distribution is calculated from the experimental O atom velocity distribution[63] by the methods outlined in Refs. 65 and 67. In the present work, we fitted the expression

$$f(x)=(a_0+a_1x+a_2x^2+a_3x^3)\exp(-bx^2), \tag{9}$$

where $x=E_{\mathrm{coll}}$, to 500 points from the distribution used in Ref. 33. A very accurate fit was obtained, with a standard deviation of less than 2×10^{-4} for the function which is scaled such that its maximum value is 1.0. The distribution decreases to a magnitude less than 10^{-5} for $E_{\mathrm{coll}} \geqslant 11.0$ kcal/mol, which is why higher collision energies were not considered in the present calculations.

D. Product Rotational Distributions

The main quantities in this study that can be compared to experimental observations are the rotational distributions of the product OH molecules. In QCT simulations, the rotational quantum number of the product molecule is found by equating the rotational angular momentum to $j'(j'+1)\hbar^2$ from which the (noninteger) j' is calculated. The vibrational energy is obtained as the difference between the internal energy and the rotational energy calculated from the j'. The vibrational quantum number is then calculated by equating the vibrational energy to a Dunham expression for the diatomic. The rotational distributions at each vibrational level populated is accumulated by a binning scheme in which the non-integer value of j' is rounded to the nearest integer. The product rotational distribution obtained in this fashion at each energy is multiplied by the factor $f(E_{\rm coll})$ calculated from Eq. (9), and added together to get the total product rotational distribution observed in the experiment. In other words, we accumulate

$$F(v',j')=\sum_{i=1} f(E_{{\rm coll},i})N_r(v',j';E_{{\rm coll},i}), \tag{10}$$

where N_r is the number of reactive trajectories in the state (v',j') out of the total number N propagated at the collision energy $E_{{\rm coll},i}$. Finally, these accumulated rotational distributions are normalized by dividing them by the sum of the distributions in the OH $v'=0$ and $v'=1$ manifolds, as done in the case of the experimental results of Zhang *et al.*,[21] to yield the distributions

$$P(v',j')=\frac{F(v',j')}{F_{\rm tot}}, \tag{11}$$

where $F_{\rm tot}=\Sigma_{j'}[F(0,j')+F(1,j')]$. The statistical error in these distributions is evaluated as[60]

$$\Delta P(v',j')=\frac{F(v',j')}{F_{\rm tot}}\left(\frac{F_{\rm tot}-F(v',j')}{F_{\rm tot}F(v',j')}\right)^{1/2}. \tag{12}$$

The quantities $P(v',j')\pm\Delta P(v',j')$ are compared to the experimental distributions.

III. RESULTS

The results of the QCT calculations are presented in this section and compared to the experimental results in Ref. 21 where appropriate. The total reaction cross section $\sigma^R_{v,j}(E_{\rm coll})$ from QCT calculations is calculated as

$$\sigma^R_{v,j}(E_{\rm coll})=\pi b^2_{\rm max}\frac{N_r}{N},$$

where N_r is the total number of reactive trajectories out of the total N propagated at a specific collision energy. The statistical error in the cross sections is evaluated as[60]

$$\Delta\sigma^R_{v,j}(E_{\rm coll})=\pi b^2_{\rm max}\frac{N_r}{N}\left(\frac{N-N_r}{NN_r}\right)^{1/2}.$$

The $\sigma^R_{v,j}(E_{\rm coll})$ for the three initial states considered are plotted as functions of the collision energy in Fig. 3. Figure 3(a) shows the full range of collision energies examined while Figure 3(b) provides a magnified view of the near-threshold region. Also shown in Fig. 3(a) is the collision energy distribution function used to weight the rotational distributions, calculated using Eq. (9).

It is interesting to contrast the behavior of the reaction cross sections on the S4 surface to those calculated by Aoiz *et al.*,[33] on the KSG surface. There appear to be no clear trend in the classical threshold behavior for this reaction on either potential surface. On the S4 surface, the reaction initiated in the HCl $(v,j)=(2,1)$ state yields a nonzero reaction cross section for $E_{\rm coll}\geqslant 0.4$ kcal/mol. The classical reaction thresholds for reaction initiated in the (2,6) and (2,9) states occur, respectively, at collision energies of 0.7 and 0.3 kcal/mol. On the other hand, on the KSG surface, the HCl $(v,j)=(2,1)$ state is unreactive for collision energies less than 1.55 kcal/mol (0.069 eV), while the thresholds for the (2,6) and (2,9) states occur, respectively, at collision energies of approximately 1.27 kcal/mol (0.055 eV) and 1.50 kcal/mol (0.065 eV). The much higher classical reaction thresholds on the KSG surface, in spite of the lower reaction barrier, is suggestive of a higher degree to which vibrational adiabatic-

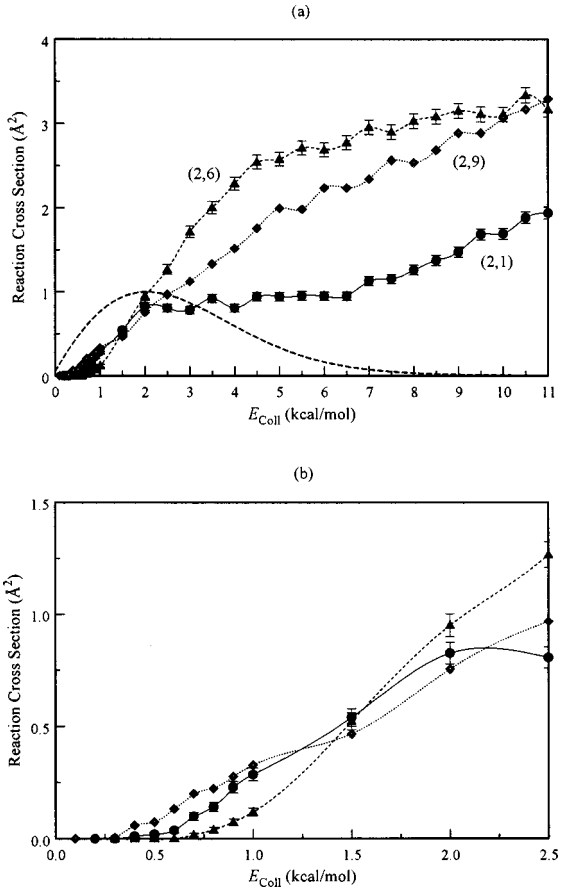

FIG. 3. The total reaction cross section as a function of collision energy for reactions initiated in the HCl $(v=2, j=1, 6, 9)$ states. Panel (a) shows the full range of collision energies examined as well as the broad collision energy distribution used to weight the cross-sections when computing the product rotational distributions. Panel (b) expands the low energy region to reveal some details of the near-threshold behavior. The symbols represent the energies at which the QCT calculations were carried out, and the lines are spline interpolations through them. For each initial state, 10 000 trajectories were propagated at each energy.

ity is preserved on that surface as the three particles approach each other.

An important difference between the reaction cross-sections calculated on the S4 and KSG surfaces lies in the marked *increase* in reactivity on the S4 surface with rotational excitation of the reagent molecule compared to a marked *decrease* on the KSG surface. As evident from Fig. 3, $\sigma^R_{2,1}$ is the smallest of the three curves plotted at nearly all collision energies examined. Also, $\sigma^R_{2,6}$ is greater than $\sigma^R_{2,9}$ except at the lowest and highest collision energies. There is, however, a suggestion from Fig. 3(a) that for $E_{\text{coll}}>11.0$ kcal/mol, the (2,9) state may have a higher reaction cross section. An average of the reaction cross sections $\sigma^R_{v,j}$ over the collision energies examined, weighted by the collision energy distribution function,

$$\langle \sigma^R_{v,j} \rangle = \pi b^2_{\max} \sum_{i=1} f(E_{\text{coll},i}) \frac{N_r}{N} \left[\sum_{i=1} f(E_{\text{coll},i}) \right]^{-1}$$

yields 0.6043, 1.2692, and 0.8504 Å ^{2} respectively, for the initial states $j=1, 6, 9$. This means that the average cross-section increases by a factor of 2.1 between $j=1$ and $j=6$ and by a factor of 1.41 between $j=1$ and $j=9$. This enhancement of reactivity with rotational excitation of HCl appears to be in agreement with the observation of Zhang *et al.*[21] that the experimental reaction cross section increases by a factor of 1.5 ± 0.5 as j increases from 1 to 9. An earlier report from the Zare group[20] had indicated that this increase is not necessarily monotonic with j. These observations are in excellent agreement with the present results. A similar trend ($\sigma^R_{2,1}<\sigma^R_{2,9}<\sigma^R_{2,6}$) in reaction cross sections were observed also on the S1 surface[34] where calculations were limited to a single collision energy.

The OH rotational distributions resulting from the reaction of O(^3P) with HCl($v=2, j=1, 6, 9$) are shown in Figs. 4–6. The rotational distribution in the OH $v'=0$ manifold is shown in the panel (a) of these figures while that in the $v'=1$ manifold is presented in panels (b). The QCT rotational distributions, represented as empty circles connected by solid lines, are compiled and normalized as described in the preceding section. Also shown in these figures are the experimental distributions observed by Zhang *et al.*, taken from Ref. 21, and represented as solid circles connected by dashed lines. The errors in the experimental distributions have been reported to be about 10% of the value of the distribution in each case. The statistical errors from the QCT calculations, which depend mainly on the number of trajectories propagated and the number of reactive trajectories accumulated, are calculated using Eq. (12) and are also shown in the figures. The QCT errors in the present work are, on average, about an order of magnitude smaller than those reported in our earlier work on the S1 surface.[34]

The most important observation to be made from Fig. 4(a) is that the QCT calculations appear to reproduce the experimentally observed nonmonotonic rise in the rotational distribution. The QCT distribution has a peak at $j'=10$ and a dip at $j'=11$, in nearly perfect agreement with the experimental results. However, the absolute magnitudes of the QCT distribution at these values of j' are only about 50% of the experimental results. Also, the dominant part of the QCT

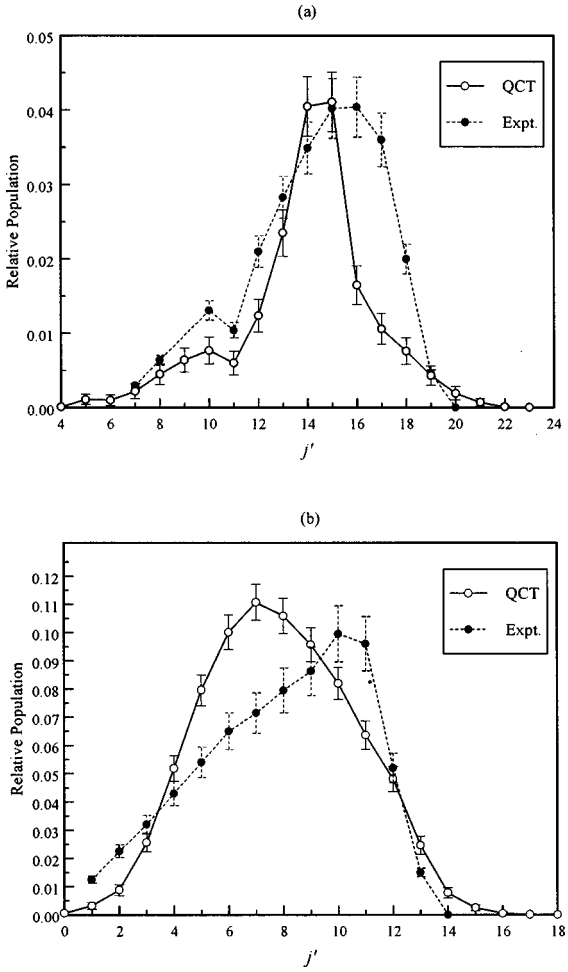

FIG. 4. The OH rotational distributions for reactions initiated in the HCl ($v=2, j=1$) state. Panels (a) and (b) compare the QCT and experimental distributions for OH ($v'=0$) and ($v'=1$), respectively. The QCT distributions are compiled from propagating a total of 270 000 trajectories, weighted by the collision energy distribution function of Fig. 3(a) and normalized as described in text. The experimental results are taken from Ref. 21.

distribution spans an extremely narrow range of j', although it appears to be superimposed on a broader distribution that spans a slightly larger range of j' values than the experimental distribution. The QCT distribution shown in Fig. 4(b) only has a qualitative similarity to the experimental distribution. The QCT distribution peaks at $j'=7$ while the experimental one peaks at $j'=10$. However, the QCT and experimental distributions have similar average magnitudes and span a similar range of j' values.

It is clear from Fig. 5(a) that the QCT results do not reproduce the nonmonotonic behavior of the experimental rotational distribution in this case. However, the QCT distribution for $j'>11$ is, in fact, in relatively good agreement with the experimental distribution. Both distributions peak at nearly the same j' and are rather similar in their overall shape. The QCT and experimental distributions in Fig. 5(b) shows the same 3 rotational quanta discrepancy in the location of the peak of the distribution observed in Fig. 4(b). Once again, the two distributions have similar relative magnitudes and span similar ranges of j'.

The QCT rotational distribution of Fig. 6(a) is in excel-

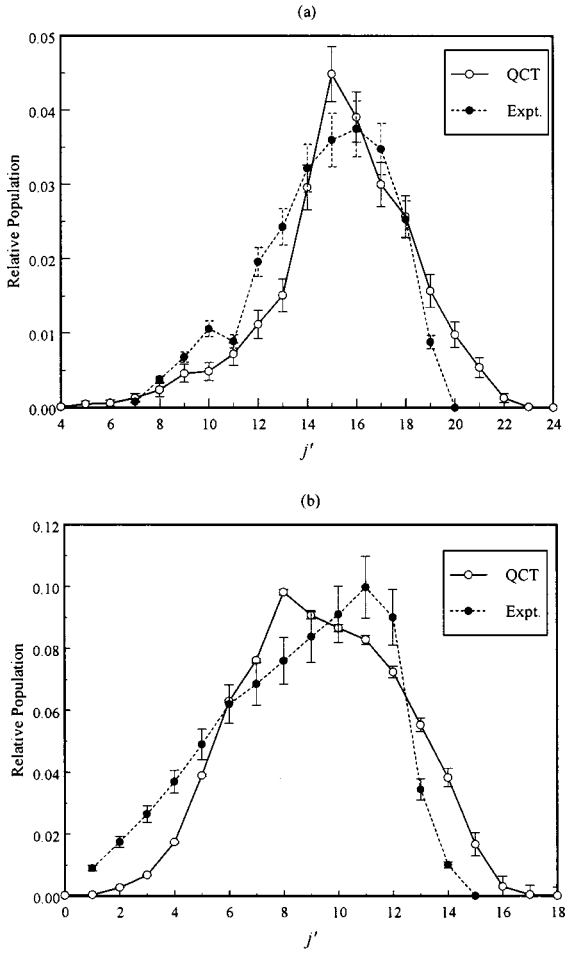

FIG. 5. Same as Fig. 4, but for the HCl ($v=2, j=6$) initial state. The QCT distributions are compiled from propagating a total of 230 000 trajectories.

lent agreement with the experimental distribution except for the fact that the former appears to be shifted about 2 rotational quanta to the right. The shoulder observed in the experimental distribution at $j'=9-10$ is present in the QCT distribution at $j'=12-13$, at nearly the same magnitude. The QCT distribution, in this case, peaks at a higher value of j' than the experimental one and shows an interesting steplike structure at $j'=19-20$. The two distributions plotted in Fig. 6(b), on the other hand, are once again different from each other in nearly identical ways that the distributions in Figs. 4(b) and 5(b) were, including the 3 rotational quanta difference in the relative positions of the peaks of the distributions.

In spite of the differences between the QCT and experimental rotational distributions, it is clear that the QCT dynamics on the S4 surface accounts for the high degree of rotational excitation of products and the significant branching to the OH $v'=0$ manifold observed experimentally. In examining the rotational distributions more closely, it was found that the behavior at the lower values of j' was dominated by reactive trajectories at lower collision energies. In particular, the reactive trajectories at $E_{\mathrm{coll}}\simeq 3.0$ kcal/mol were found to yield rotational distributions which displayed striking qualitative similarities to the experimental distributions for $j'<14$. This becomes clear upon examining Fig. 7, where the energy dependence of the OH ($v'=0$) rotational distributions from the three initial states are presented. The quantities plotted are the ''unnormalized'' $F(v',j')$ quantities of Eq. (10), and the damping influence of the collision energy distribution is clearly visible as one approaches higher collision energies. In plotting these distributions, we have interpolated between data points using splines to get roughly twice the number of grid points in each direction as there are data points. However, care has been taken to ensure that spurious structures have not been ''created'' as a result of this interpolation. In each panel, the distribution at $E_{\mathrm{coll}}=3.0$ kcal/mol is highlighted by a thick line. It is clear from Fig. 7(a) that the structure in the QCT $F(0,j')$ distribution from the HCl (2,1) state arises mainly from collision energies in the vicinity of 3.0 kcal/mol. It is also clear that the shoulders in the rotational distributions resulting from the (2,6) and (2,9) initial states also are due to the dynamics of the reaction near this collision energy. It is especially interesting that the distribution at $E_{\mathrm{coll}}=3.0$ kcal/mol in Fig. 7(b) shows some evidence of a peak at $j'\simeq 9$ followed by a weak trough at $j'=10-11$. However, as evident from Fig. 5(a), this structure gets averaged out when all collision energies are taken into account. In this context, it is important to point out that, although the QCT $P(0,j')$ at $E_{\mathrm{coll}}=3.0$ kcal/mol

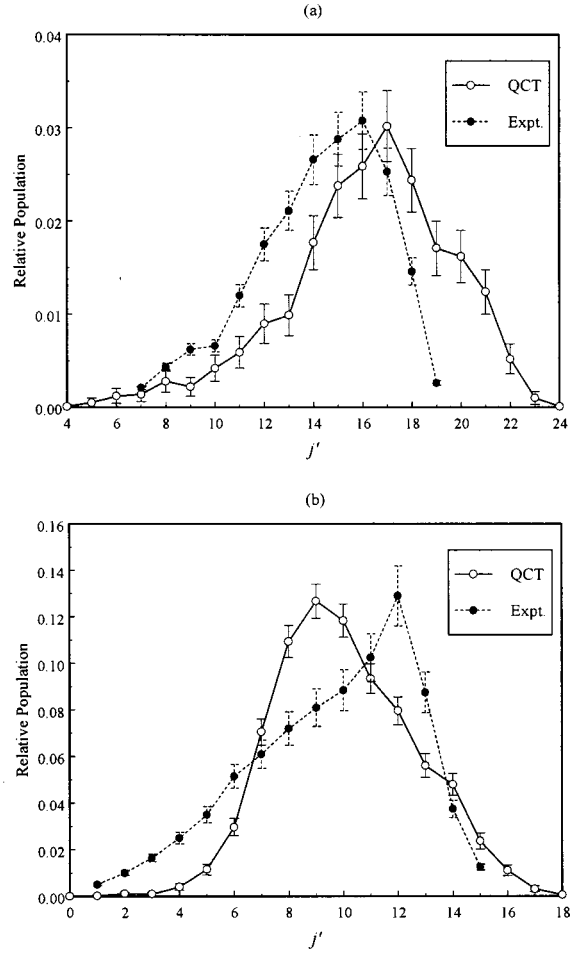

FIG. 6. Same as Figs. 4 and 5, but for the HCl ($v=2, j=9$) initial state. The QCT distributions are compiled from propagating a total of 280 000 trajectories.

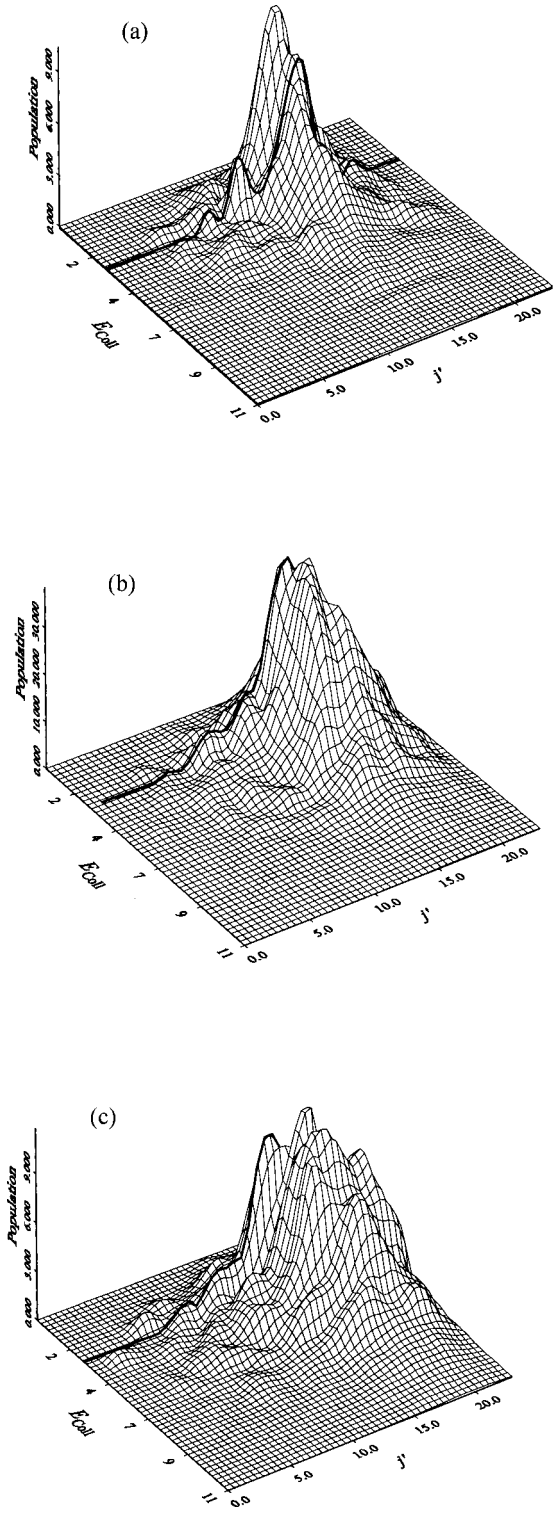

FIG. 7. The energy dependence of OH ($v'=0$) rotational distributions. The distribution at Ecoll = 3.0 kcal/mol is highlighted using thick lines. The mesh plotted is spline-interpolated to yield roughly twice the number of grid points as data in each direction. Distributions from (a) ($v=2, j=1$), (b) ($v=2, j=6$), and (c) ($v=2, j=9$) states of HCl are shown. At 3.0 kcal/mol, these bear qualitative similarities to the experimental results in Ref. 21.

shows qualitative similarities to the experimental distributions for smaller values of j', the shapes of the QCT distributions at this energy for higher values of j' are in much poorer agreement with experiment than the overall distributions plotted in Figs. 4–6. Therefore, the contribution to $P(0,j')$ from the other collision energies are important in determining the shape of the overall distribution, particularly for $j' \geqslant 14$.

It was mentioned above that the QCT dynamics accounts for the experimentally observed high degree of vibrational branching to the OH $v'=0$ manifold. This is a relevant observation because of the fact that access to the OH $v'=1$ manifold is energetically much more favorable from the $v=2$ states of HCl. Populating the $v'=0$ states requires the conversion of a considerable amount of vibrational energy into rotational or translational energy. It is also interesting that no OH $v'=0$ product was observed in the case of the O(^3P)+HBr reaction.[68] Zhang *et al.* found that in the case of the O(^3P)+HCl reaction, the ratio OH($v'=1$)/OH($v'=0$) was $2.6\pm0.1, 3.0\pm0.1$, and 4.1 ± 0.2 for the initial states $j=1, 6$ and 9, respectively. Interestingly, no $v'=2$ product was detected in the experiments. Vibrational ratios obtained from QCT calculations need to be interpreted with some caution since zero point energy is not conserved in these calculations. Also, the vibrational quantum number calculated from the vibrational energy could, in some instances, turn out to have a negative value. Therefore, all trajectories with $v'<0.5$ are assigned to the $v'=0$ level, those with $0.5 \leqslant v' < 1.5$ to $v'=1$ and those with $1.5 \leqslant v' < 2.5$ to $v'=2$. Because of this assignment of vibrational quantum numbers, several trajectories with v' values between 1.5 and 2.0 are assigned to $v'=2$ in the QCT calculations. Keeping these limitations of the QCT method in mind, we have computed collision energy weighted vibrational branching ratios as

$$R_j = \frac{\sum_i f(E_{\mathrm{coll},i}) \sum_{j'} P(1,j')}{\sum_i f(E_{\mathrm{coll},i}) \sum_{j'} P(0,j')},$$

for each initial state j. These calculations yield ratios of 4.30, 3.00, and 3.73 for $j=1, 6$ and 9, respectively. These numbers are higher than the ratios 1.52, 1.45 and 1.38 calculated on the KSG surface[33] and, at least for the case of (2,6) and (2,9) states, in better agreement with the experimental observations.

IV. SUMMARY AND CONCLUSIONS

This work presents a new potential energy surface, called the S4 surface, for the lowest $^3A''$ state for the O(^3P)+HCl→OH+Cl reaction, based on SEC scaled *ab initio* data at the MR-CI+Q level of theory. As can be seen from Fig. 1, this potential energy surface is physically reasonable for total energies below 42 kcal/mol. Above this energy, the H+ClO channel which is not represented in the S4 surface would, presumably, become accessible to the reagents. Below this energy, however, the potential surface appears to be quite faithful to the underlying data as evidenced by the low rms error of the fit (0.48 kcal/mol) and the comparison of the fit to *ab initio* data calculated *a posteriori*, as shown in Figs. 2. The presence of two van der Waals minima, one each in the entrance and exit channels, makes

the minimum energy reaction path quite complicated in configuration space. If one were to follow the minimum energy path, the reagents would approach at a collinear geometry, sampling the shallow entrance channel well. The three-atom system would then assume a bent configuration to cross the reaction barrier at an O–H–Cl angle of 131.4°, followed by a rapid decrease of this angle to 80.4° as the system falls into the deep exit channel well. This bending motion could impart a considerable amount of rotational energy to the OH fragment and could account for the high rotational excitation observed in the experiments and QCT calculations even in for reagents prepared in the $v=2$ state.

We have studied the classical dynamics of the reaction of $O(^3P)+HCl(v=2;j=1,6,9)$ at several collision energies from the reaction threshold to 11.0 kcal/mol. The distribution of collision energies expected to be present in the experiments of Zhang *et al.*,[21] has been included in the analysis of the results so that direct comparison of QCT results to experimentally observed quantities such as total reaction cross sections and product rotational distributions could be made. These comparisons indicate that the S4 surface is capable of reproducing many of the experimental observations, at least qualitatively. For instance, the S4 surface appears to predict a significant enhancement of reaction cross section due to rotational excitation of the reagent molecule, in keeping with experimental observations. This is in marked contrast with the exactly opposite behavior observed for the KSG surface, where rotational excitation of HCl was found to result in a marked decrease in the magnitude of the reaction cross section. It was also found that, in spite of the lower reaction barrier, the classical reaction thresholds for reactions from the HCl $(v=2)$ states were higher on the KSG surface than the S4 surface, presumably due to better preservation of vibrational adiabaticity on the former.

The QCT product rotational distributions $P(v',j')$ in the $OH(v'=0)$ manifold for the HCl $(v=2,j=1)$ state on the S4 surface show the non-monotonic behavior observed in the experiments even after the distributions are averaged over the full range of collision energies studied. In the case of the HCl $(v=2,j=6)$ state, oscillations qualitatively similar to those observed experimentally are present in the QCT $P(0,j')$ near $E_{\mathrm{coll}}\simeq 3.0$ kcal/mol but these, being much less pronounced than those in the $(v=2,j=1)$ case, tend to get ''smoothed out'' into a broad shoulder when all collision energies are considered. The QCT $P(0,j')$ resulting from the HCl $(v=2,j=9)$ on the other hand, appears to have qualitatively the same shape as the experimental distribution, but appears to be too ''hot'' by about one or two rotational quanta. An examination of the energy dependence of the rotational distributions in the OH $v'=0$ manifold shows that the shapes of the distributions at lower j' are mainly determined by reactive trajectories at low collision energies. The QCT rotational distributions in the $v'=1$ manifold for all three initial states examined is observed to peak at value of j' too low by 3 rotational quanta compared to the corresponding experimental distribution. However, there are important qualitative similarities between the QCT and experimental rotational distributions. The S4 surface accounts for the experimentally observed high rotational excitation of the OH molecules. Moreover, in spite of the *independent* normalizations of the QCT and experimental rotational distributions, they appear to have very similar average magnitudes and span approximately the same range of j' values.

Although the QCT vibrational branching ratios have to be interpreted with some caution, those calculated on the S4 surface for the initial states (2,6) and (2,9) of HCl are in better agreement with the experimental results than those obtained on the KSG surface. However, the ratio calculated for the (2,1) state on the S4 surface is higher than the other two and, therefore, the overall trend of vibrational branching ratios with increasing j quantum number is at odds with experiment.

One question not addressed in the present study or that of Aoiz *et al.* is the role of the $^3A'$ electronic state in this reaction. This state becomes degenerate with the $^3A''$ state at asymptotic and collinear geometries, but appears to lie above it at other geometries. This means that the minimum energy reaction barrier on the $^3A'$ surface should coincide with the collinear saddle point on the present surface. This barrier height is 12.95 kcal/mol, which rules out the possibility of the upper surface having significant contributions to the thermal rate coefficients at $T\leqslant 1000$ K. However, the energies probed in the present study as well as the experiments of Zhang *et al.*, lie well above the barrier height on the $^3A'$ surface. Therefore, there is still a possibility that the experimentally observed product rotational distributions, total cross sections, and vibrational branching ratios could be influenced by the dynamics on the $^3A'$ surface. We are, at present, exploring this possibility using a LEPS model surface constructed based on the geometry of the S4 surface at $\theta_{\mathrm{OHCl}}=180°$, and the angular dependence of the $^3A'$ surface at $(r^{\ddagger}_{\mathrm{OH}},r^{\ddagger}_{\mathrm{HCl}})$, obtained from SEC-scaled *ab initio* calculations.

ACKNOWLEDGMENTS

This research is supported by a grant to B.R. from the Louisiana Education Quality Support Fund, under Contract No. LEQSF (1994-97)-RD-A-18 and the National Science Foundation, Grant No. CHE 97-12764. R.E.W. acknowledges support from the National Science Foundation and the Welch Foundation. We are extremely grateful to Professors Javier Aoiz and Luis Bañares for sending us a preprint of Ref. 33 and also providing us with the numerical values of the collision energy distribution shown in Fig. 3(a) at several collision energies.

[1] H. S. Johnston, Annu. Rev. Phys. Chem. **43**, 1 (1992).
[2] I. W. M. Smith, in *Bimolecular Collisions* (*Advances in Gas-Phase Photochemistry and Kinetics*), edited by M. N. R. Ashfold and J. E. Baggott (Royal Society of Chemistry, Letchworth, 1989).
[3] V. P. Balakhnin, V. I. Egorov, and E. I. Intezarova, Kinet. Katal. **12**, 299 (1971); **12**, 258 (1971).
[4] E. L. Wong and F. E. Belles, NASA Tech. Note D-6495 (1975); Chem. Abs. **76**, 18326q (1972).
[5] D. Singleton and R. Cvetanovic, Int. J. Chem. Kinet. **13**, 301 (1975).
[6] R. D. H. Brown, G. P. Glass, and I. W. M. Smith, Chem. Phys. Lett. **32**, 517 (1975).
[7] R. D. H. Brown and I. W. M. Smith, Int. J. Chem. Kinet. **7**, 301 (1975).
[8] A. R. Ravisankara, G. Smith, R. T. Watson, and D. D. Davis, J. Phys. Chem. **81**, 2220 (1977).
[9] W. Hack, G. Mex, and H. G. Wagner, Ber. Bunsenges. Phys. Chem. **81**, 677 (1977).

[10] C. Park, J. Phys. Chem. **81**, 499 (1977).
[11] J. E. Butler, J. W. Hudgens, M. C. Lin, and I. W. M. Smith, Chem. Phys. Lett. **58**, 216 (1978).
[12] D. L. Baulch, J. Duxbury, S. J. Grant, and D. C. Montague, J. Phys. Chem. Ref. Data **10**, 1 (1981).
[13] D. L. Baulch, R. A. Cox, R. F. Hampton, Jr., J. A. Kerr, J. Troe, and R. T. Watson, J. Phys. Chem. Ref. Data **13**, 1259 (1984).
[14] K. Mahmud, J. S. Kim, and A. Fontijn, J. Phys. Chem. **94**, 2994 (1990).
[15] D. Arnoldi and J. Wolfrum, Chem. Phys. Lett. **24**, 234 (1974).
[16] R. D. H. Brown, G. P. Glass, and I. W. M. Smith, Chem. Phys. Lett. **32**, 517 (1975).
[17] Z. Karny, B. Kartz, and A. Szoke, Chem. Phys. Lett. **35**, 100 (1975).
[18] R. G. MacDonald and C. B. Moore, J. Chem. Phys. **68**, 513 (1978).
[19] M. Kneba and J. Wolfrum, *Proceedings of the 17th International Symposium on Combustion* (Combustion Institute, Pittsburg, 1978), p. 497.
[20] R. J. Rakestraw, K. G. McKendrick, and R. N. Zare, J. Chem. Phys. **87**, 7341 (1987).
[21] R. Zhang, W. J. van der Zande, M. J. Bronikowski, and R. N. Zare, J. Chem. Phys. **94**, 2704 (1991).
[22] R. D. Brown and I. W. M. Smith, Int. J. Chem. Kinet. **10**, 1 (1978).
[23] A. Persky and M. Broida, J. Chem. Phys. **81**, 4352 (1984).
[24] H. Koizumi and G. C. Schatz, Int. J. Quantum Chem. **23**, 137 (1989); in *Advances in Molecular Vibration and Collision Dynamics*, edited by J. M. Bowman and M. A. Ratner (JAI, Greenwich, CT, 1990).
[25] S. C. Park, H. Nakamura, and A. Ohsaki, J. Chem. Phys. **92**, 6538 (1990).
[26] M. S. Gordon, K. K. Baldridge, D. E. Bernholdt, and R. J. Bartlett, Chem. Phys. Lett. **158**, 189 (1989).
[27] H. Koizumi, G. C. Schatz, and M. S. Gordon, J. Chem. Phys. **95**, 6421 (1991).
[28] K. Moribayashi and H. Nakamura, J. Phys. Chem. **99**, 15410 (1995).
[29] W. H. Thompson and W. H. Miller, J. Chem. Phys. **106**, 142 (1997); **107**, 2164 (1997).
[30] K. Nobusada, K. Moribayashi, and H. Nakamura, J. Chem. Soc., Faraday Trans. **93**, 721 (1997).
[31] B. Poirier, J. Chem. Phys. **108**, 5216 (1998).
[32] F. Matzkies and U. Manthe, J. Chem. Phys. **110**, 88 (1999).
[33] F. J. Aoiz, L. Bañares, J. F. Castillo, M. Menéndez, and J. E. Verdasco, PCCP **1**, 1149 (1999).
[34] B. Ramachandran, J. Senekowitsch, and R. E. Wyatt, Chem. Phys. Lett. **270**, 387 (1997).
[35] T. C. Allison, B. Ramachandran, J. Senekowitsch, D. G. Truhlar, and R. E. Wyatt, J. Mol. Struct.: THEOCHEM **454**, 307 (1998).
[36] D. G. Truhlar, A. D. Issacson, and B. C. Garrett, in *Theory of Chemical Reaction Dynamics*, edited by M. Baer (CRC Press, Boca Raton, FL, 1985), and references therein.
[37] B. C. Garrett, D. G. Truhlar, R. S. Grev, and A. W. Magnuson, J. Phys. Chem. **84**, 1730 (1980); **87**, 4554 (E) (1983).
[38] Y.-P. Liu, D.-h. Lu, A. Gonzàlez-Lafont, D. G. Truhlar, and B. C. Garrett, J. Am. Chem. Soc. **115**, 7806 (1993).
[39] T. C. Allison, B. Ramachandran, J. Senekowitsch, D. G. Truhlar, and R. E. Wyatt (work in progress).
[40] R. N. Zare (private communication to B.R.).
[41] F. J. Aoiz, V. J. Herrero, and V. Sáez Rábanos, J. Phys. Chem. **97**, 7423 (1992).
[42] F. J. Aoiz, L. Bañares, V. J. Herrero, V. Séz Rábanos, L. Schneider, and R. E. Wyatt, J. Chem. Phys. **101**, 5781 (1994).
[43] L. Schnieder, K. Seekamp-Rahn, J. Borkowski, E. Wrede, K. H. Welge, F. J. Aoiz, L. Bañares, M. J. D'Mello, V. Sáez Rábanos, and R. E. Wyatt, Science **269**, 207 (1995).
[44] F. J. Aoiz, L. Bañares, T. Diez-Rojo, V. J. Herrero, and V. Sáez Rábanos, J. Phys. Chem. **100**, 4071 (1996).
[45] F. J. Aoiz, M. T. Martinez, M. Menéndez, V. Sáez Rábanos and J. E. Verdasco, Chem. Phys. Lett. **299**, 25 (1999).
[46] MOLPRO92 is a package of quantum chemistry programs written by H.-J. Werner and P. J. Knowles with contributions from J. Almlöf, R. Amos, S. Elbert, K. Hampel, W. Meyer, K. Peterson, R. Pitzer, and A. Stone. The current version of this program is MOLPRO96.
[47] H.-J. Werner and P. J. Knowles, J. Chem. Phys. **89**, 5803 (1989); P. J. Knowles and H.-J. Werner, Chem. Phys. Lett. **145**, 514 (1988).
[48] T. H. Dunning, J. Chem. Phys. **90**, 1007 (1989).
[49] S. R. Langhoff and E. R. Davidson, Int. J. Quantum Chem. **8**, 61 (1974).
[50] M. R. A. Blomberg and P. E. M. Seigbahn, J. Chem. Phys. **78**, 5803 (1983); J. Simons, J. Phys. Chem. **93**, 626 (1989).
[51] F. B. Brown and D. G. Truhlar, Chem. Phys. Lett. **117**, 307 (1985).
[52] D. W. Schwenke, R. Steckler, F. B. Brown, and D. G. Truhlar, J. Chem. Phys. **84**, 5706 (1986); C.-h. Yu, D. J. Kouri, M. Zhao, D. G. Truhlar, and D. W. Schwenke, Chem. Phys. Lett. **157**, 491 (1989); G. C. Lynch, R. Steckler, D. W. Schwenke, A. J. C. Varandas, D. G. Truhlar, and B. C. Garrett, J. Chem. Phys. **74**, 7136 (1991).
[53] S. L. Mielke, G. C. Lynch, D. G. Truhlar, and D. W. Schwenke, Chem. Phys. Lett. **213**, 10 (1993); **217**, 173 (1994).
[54] D. W. Schwenke, S. C. Tucker, R. Steckler, F. B. Brown, G. C. Lynch, and D. G. Truhlar, J. Chem. Phys. **90**, 3110 (1989).
[55] A. J. C. Varandas, J. Chem. Phys. **90**, 4379 (1989).
[56] H. Zhang, B. Ramachandran, J. Senekowitsch, and R. E. Wyatt, J. Mol. Struct: THEOCHEM (to be published).
[57] E. Garcia and A. Laganá, Mol. Phys. **56**, 621 (1985).
[58] K. P. Huber and G. Herzberg, *Constants of Diatomic Molecules*, (Van Nostrand Reinhold, New York, 1979).
[59] A. Aguado and M. Paniagua, J. Chem. Phys. **96**, 1265 (1992).
[60] J. T. Muckerman and D. G. Truhlar, in *Atom-Molecule Collision Theory: A Guide to the Experimentalist*, edited by R. B. Bernstein (Plenum, New York, 1979).
[61] M. B. Faist, J. T. Muckerman, and F. E. Schubert, J. Chem. Phys. **69**, 4087 (1978).
[62] In Ref. 34, the units of $b_{\max}$ and the reaction cross section $\sigma^R_{v,j}$ were erroneously reported as a_0 and a_0^2, respectively.
[63] V. P. Hradil, T. Suzuki, S. A. Hewitt, P. L. Houston, and B. J. Whitaker, J. Chem. Phys. **99**, 4455 (1993).
[64] W. J. van der Zande, R. Zhang, R. N. Zare, K. G. McKendrick, and J. J. Valentini, J. Phys. Chem. **95**, 8205 (1991).
[65] M. Brouard, S. P. Duxon, P. A. Enriquez, and J. P. Simons, J. Chem. Phys. **97**, 7414 (1992).
[66] F. J. Aoiz, M. Brouard, P. A. Enriquez, and R. Sayos, J. Chem. Soc., Faraday Trans. **89**, 1427 (1993).
[67] E. P. Gilbert, G. Maitland, A. Watson, and K. G. McKendrick, J. Chem. Soc., Faraday Trans. **89**, 1527 (1993).
[68] K. G. McKendrick, D. J. Rakestraw, and R. N. Zare, J. Phys. Chem. **92**, 5530 (1988).